Hierarchical complexity of the macro-scale neonatal brain

Manuel Blesa[a,*], Paola Galdi[a], Simon R. Cox[b], Gemma Sullivan[a], David Q. Stoye[a], Gillian J. Lamb[a], Alan J. Quigley[c], Michael J. Thrippleton[d,e], Javier Escudero[e], Mark E. Bastin[d], Keith M. Smith[f,g,1], James P. Boardman[a,d,1]

[a]*MRC Centre for Reproductive Health, University of Edinburgh, Edinburgh EH16 4TJ, UK*
[b]*Lothian Birth Cohorts group, Department of Psychology, University of Edinburgh, Edinburgh EH8 9JZ, UK*
[c]*Department of Radiology, Royal Hospital for Sick Children, Edinburgh EH9 1LF, UK*
[d]*Centre for Clinical Brain Sciences, University of Edinburgh, Edinburgh EH16 4SB, UK*
[e]*School of Engineering, Institute for Digital Communications, University of Edinburgh, Edinburgh EH9 3FG, UK*
[f]*Usher Institute, University of Edinburgh, Edinburgh EH16 4UX, UK*
[g]*Health Data Research UK, London NW1 2BE, UK*

Abstract

The human adult structural connectome has a rich topology composed of nodal hierarchies containing highly diverse connectivity patterns, aligned to the diverse range of functional specialisations in the brain. The emergence of this hierarchical complexity in human development is unknown. Here, we substantiate the hierarchical tiers and complexity of brain networks in the newborn period, assess correspondences with hierarchical complexity in adulthood, and investigate the effect of preterm birth, a leading cause of neurocognitive impairment and atypical brain development, on hierarchical complexity. We report that the neonatal and adult structural connectomes are both composed of distinct hierarchical tiers. Consistency of ROIs is found at both ends of this hierarchy during early life and in adulthood, but significant differences are evident in intermediate tiers. The neonatal connectome is hierarchically complex in term born neonates, but hierarchically complexity is altered in association with preterm birth. This is mainly due to diversity of connectivity patterns in Tier 3, which is comprised of regions that underlie sensorimotor processing and its integration with cognitive information. For neonates and adults, the highest tier (comprising hub regions) is ordered, rather than complex, with more homogeneous connectivity patterns in structural hubs. This suggests that the brain develops first a more rigid hierarchical structure in hub regions allowing for the development of greater and more diverse functional specialisation in lower level regions, while connectivity underpinning this diversity is dysmature in infants born preterm.

1. Introduction

The integrity of brain development during pregnancy and the newborn period is critical for life long cognitive function and brain health. During the second and third trimesters of pregnancy, there is a phase of rapid brain maturation characterised by volumetric growth, increases in cortical complexity, white matter organization and myelination [1]. Early exposure to extrauterine life due to preterm birth affects around 11% of births, and is closely associated with neurodevelopmental, cognitive and psychiatric impairment [2, 3, 4], and alterations to development [5] that are apparent using *in vivo* imaging techniques. At the macro scale, these alterations can be characterised by charting white matter connections between brain regions using diffusion MRI (dMRI) [6, 7, 8, 9, 10, 11, 12].

Several metrics that are found ubiquitously in real-world networks have been used to model brain connectivity in the neonatal brain, including local and global efficiency, small-worldness, clustering coefficient,

*Correspondence: Manuel Blesa, Queen's Medical Research Institute, 47 Little France Crescent, Edinburgh EH16 4TJ, UK. Email: manuel.blesa@ed.ac.uk
[1]These authors contributed equally to the work.

characteristic path length and rich club coefficient [7, 8, 9, 11, 13], and often they reveal remarkable structural and functional architectural facsimiles between the newborn and adult brain [13, 14, 15]. Hierarchical complexity (HC) is a measure of the diversity of connectivity patterns found across hierarchically equivalent (same degree) network nodes, and it reflects the hierarchical and functionally diverse capacities of the human brain. HC provides a tractable signature of brain network architecture in the adult connectome [16, 17]: four hierarchical tiers broadly comprise different categories of functional processing – cognitive, sensorimotor, integrative, and memory and emotion [16]. To investigate the possibility that HC is established in the perinatal period, and that alterations in HC patterning might characterize atypical brain development in preterm infants, we have developed an approach to assess HC in the newborn period.

We used the approach to define the hierarchical structure of the connectomes of a cohort of neonates. We investigated similarities and differences in HC between birth and adulthood, and we explored the effect of preterm birth on HC in the newborn period. We report that the newborn structural connectome is highly organised into separable hierarchical tiers; that global HC is larger in adulthood compared to infancy; and that early exposure to extrauterine life by preterm birth leads to differences in HC that are largely driven by a single tier, which contains ROIs concerned with the integration of high order cognitive information and sensorimotor processing.

2. Material and methods

2.1. Participants and data acquisition

For the present work, two datasets were used:

- **Theirworld Edinburgh Birth Cohort (TEBC)**: Participants were recruited as part of a longitudinal study designed to investigate the effects of preterm birth on brain structure and long term outcome. The study was conducted according to the principles of the Declaration of Helsinki, and ethical approval was obtained from the UK National Research Ethics Service. Parents provided written informed consent. A total of 136 neonates (77 preterm [with gestational age at birth ¡ 32 weeks] and 59 term) underwent MRI at term equivalent age at the Edinburgh Imaging Facility: Royal Infirmary of Edinburgh, University of Edinburgh, UK.

A Siemens MAGNETOM Prisma 3 T MRI clinical scanner (Siemens Healthcare Erlangen, Germany) and 16-channel phased-array paediatric head coil were used to acquire the following imagining data: 3D T2-weighted SPACE (T2w) (voxel size = 1mm isotropic) with TE 409 ms and TR 3200 ms; and axial dMRI. dMRI data were acquired in two separate acquisitions to reduce the time needed to re-acquire any data lost to motion artefact: the first acquisition consisted of 8 baseline volumes (b = 0 s/mm^2 [b0]) and 64 volumes with b = 750 s/mm^2, the second consisted of 8 b0, 3 volumes with b = 200 s/mm^2, 6 volumes with b = 500 s/mm^2 and 64 volumes with b = 2500 s/mm^2. An optimal angular coverage for the sampling scheme was applied [18].

In addition, an acquisition of 3 b0 volumes with an inverse phase encoding direction was performed. All dMRI images were acquired using single-shot spin-echo echo planar imaging (EPI) with 2-fold simultaneous multislice and 2-fold in-plane parallel imaging acceleration and 2 mm isotropic voxels; all three dMRI acquisitions had the same parameters (TR/TE 3400/78.0 ms). Images affected by motion artefact were re-acquired multiple times as required; dMRI acquisitions were repeated if signal loss was seen in 3 or more volumes.

Infants were fed and wrapped and allowed to sleep naturally in the scanner. Pulse oximetry, electrocardiography and temperature were monitored. Flexible earplugs and neonatal earmuffs (MiniMuffs, Natus) were used for acoustic protection. All scans were supervised by a doctor or nurse trained in neonatal resuscitation.

- **Human Connectome project (HCP)**: The HCP test-retest dataset, consisting of T1-weighted and dMRI data from 45 healthy subjects. The data were acquired with a 1.25 mm isotropic voxel size; three shells with b = 1,000, 2,000 and 3,000 s/mm^2 each shell with 90 DW volumes and six non-weighted images [19].

2.2. Data preprocessing

2.2.1. Theirworld Edinburgh Birth Cohort

dMRI processing was performed as follows: for each subject the two dMRI acquisitions were first concatenated and then denoised using a Marchenko-Pastur-PCA-based algorithm [20]; eddy current, head movement and EPI geometric distortions were corrected using outlier replacement and slice-to-volume registration [21, 22, 23, 24]; bias field inhomogeneity correction was performed by calculating the bias field of the mean b0 volume and applying the correction to all the volumes [25].

The T2w images were processed using the minimal processing pipeline of the developing human connectome project (dHCP) to obtain the bias field corrected T2w, the brain masks, the tissue segmentation and the different tissue probability maps [26, 27]. For the parcellation, the ten manually labelled subjects of the M-CRIB atlas [28] were registered to the bias field corrected T2w using affine and symmetric normalization (SyN) [29], and then the registered labels of the ten atlases were merged using joint label fusion [30], resulting in a parcellation containing 84 regions of interest (ROIs). The 5 tissue type file needed to perform the tractography, was generated by combining the tissue probability maps obtained from the dHCP pipeline with the subcortical structures derived from the parcellation process (https://git.ecdf.ed.ac.uk/jbrl/neonatal-5TT). Finally, the mean b0 EPI volume of each subject was co-registered to their structural T2w volume using boundary-based registration [31], then the inverse transformation was used to propagate ROIs label and the 5 tissue type file to dMRI space.

2.2.2. Human Connectome Project

The HCP dataset was already preprocessed, as described in [32]. Briefly, dMRI data were corrected for head motion and geometrical distortions arising from eddy currents and susceptibility artifacts [33]. Finally, the dMRI were aligned to the structural T1 image. The T1w was parcellated using the Desikan-Killany parcellation [34], resulting in 84 ROIs. Using the T1w, the probability maps of the different tissues were obtained to create the 5 tissue type file [35, 36].

2.3. Tractography and network creation

Tractography was performed using constrained spherical deconvolution (CSD) [37]. For both datasets, a multi-tissue response function was calculated [38], the only difference being that for the neonatal cohort the FA threshold of the algorithm was reduced to 0.1. For each cohort, the average response functions were calculated. Then, the multi-tissue fiber orientation distribution (FOD) was calculated [39] with the average response function using a $\mathcal{L}_{\max} = 8$. For the HCP dataset three FODs were calculated (white matter (WM)/gray matter (GM)/cerebrospinal fluid (CSF)), while for the TEBC only two (WM/CSF). Finally, a joint bias field correction and multi-tissue informed log-domain intensity normalisation on the FODs images was performed [40].

Tractography was then performed with the iFOD2 algorithm [41] using anatomically-constrained tractography [42], generating 10 million of streamlines, with a minimum length of 20 mm and a maximum of 200 mm for the neonatal data and of 250 mm for the HCP dataset and a cutoff of 0.05 (default), using backtrack [42] and a dynamic seeding [43]. To be able to quantitatively assess the connectivity, SIFT2 was applied to the resulting tractograms [43].

The connectivity matrix was constructed using a robust approach, a 2 mm radial search at the end of the streamline was performed to allow the tracts to reach the GM parcellation [44, 45]. Each connectivity matrix was multiplied by their μ coefficient obtained from the SIFT2 process, because the sum of the streamline weights needs to be proportional to units of fiber density for each subject [43]. This resulted in:

$$w_{ij} = \mu \sum_{s \epsilon S_{ij}} sc_s \tag{1}$$

where w_{ij} is the total weight of the connection of the node i with the node j, μ is the coefficient obtained from SIFT2, sc_s is the SIFT2 weight of the streamline s and $s \in S_{ij}$ represents all the streamlines connecting the nodes i and j.

The resulting matrices were then thresholded to a density of 0.3 (consistent with biological evidence that the human brain has a connection density of approximately 30% [46]) and binarized.

2.4. Hierarchical complexity

The neighbourhood of a network node is the set of all nodes to which that node shares links. The neighbourhood degree sequence of the node is then the ordered sequence of degrees of the nodes neighbours, which is a particularly useful tool for studying organisational principles of networks [17]. The HC of a network, then, involves computing the variability of neighbourhood degree sequences of nodes of the same degree. This provides a measure of the diversity of connectivity patterns within the network degree hierarchy. Let $G = (V, E)$ be a graph with nodes $V = \{1, \ldots, n\}$ and links $E = \{(i, j) : i, j \in V\}$, and let $\mathcal{K} = \{k_1, \ldots, k_n\}$ be the set of degrees of G, where k_i is the number edges adjacent to node i. Further, let $\mathcal{K}_p$ be the set of nodes of degree p. For neighbourhood degree sequence $s_i^p = \{s_i^p(1), \ldots, s_i^p(p)\}$ of node i of degree p, the HC is

$$R = \frac{1}{\mathcal{D}} \sum_{\mathcal{K}_p, |\mathcal{K}_p|>1} \frac{1}{p(|\mathcal{K}_p| - 1)} \left(\sum_{j=1}^{p} \left(\sum_{i \in \mathcal{K}_p} (s_i^p(j) - \mu^p(j))^2 \right) \right) \tag{2}$$

where $\mathcal{D}$ is the number of distinct degrees in the network and $\mu^p(j)$ is the mean of the jth entries of all p length neighbourhood degree sequences [47]. For the tier-based analyses, we used degree specific HC by averaging it over a given range of degrees, i.e. the degrees within the given tier definitions.

2.4.1. Configuration models

To control for the differences in degree distribution between individual connectomes and the different populations (term- and preterm-born infants and adult), we used configuration models [48]. The configuration model fixes the number of links at each node of the null model by providing each node with a number of 'stubs', the number of which is the node's degree in the original network. Then, pairs of stubs are randomly chosen across all nodes to establish new links. This process is repeated until there are no stubs remaining, meanwhile the process is started again anytime a link is created which either attaches a node to itself or attaches two nodes which already have an established link.

2.4.2. Hierarchical tiers

Once the global connectivity patterns were assessed, we then performed a more refined analysis of HC through different degree strengths in the network. Previous work [16] split each network into four tiers based on maximum degree magnitudes, where each tier comprised a rounded 25% of degrees. The first tier comprised nodes in the top 25% of degrees in the network, the second tier comprised of nodes with the next 25% of largest degrees, and so on. In our study, however, we wished to assess whether the degree distributions would reveal such tiers directly and so chose tiers based on peaks of the group-aggregated degree distributions, Fig 1. Once tiers were defined, we implemented tier-based analysis on both the structural connectomes and their configuration models for comparison. To track the consistency of tiers across groups (preterm-born, term-born, and adult) we computed the number of times each node appeared in a given tier across participants. For each tier, Pearson's correlation coefficients were then computed across these node proportions between preterm and term, preterm and adult and term and adult.

The equation of HC required nodes to have the same degree. This was problematic in Tier 1 and Tier 2 of neonates particularly, because these generally consisted of only a few nodes tending to have different degrees. To overcome this problem, for each participant we defined m_i as the minimum degree of Tier i nodes (where $i = 1, 2$), and implemented a random sample of m_i entries of the neighbourhood degree sequences of all nodes in Tier i, enabling us to compute HC across all Tier i nodes. For each participant, this random sampling was done 100 times and the median HC was taken as the HC of that participant.

2.4.3. Hemispheric symmetry in network neighbourhoods and common connections

As a post-hoc analysis, and to characterise better the network topology and understand the results showed by HC, we investigated the effect of cross-hemisphere neighbourhood symmetry within tiers to probe deeper into the complex organisation underlying the neonatal connectomes, following the insight that higher symmetry is associated with higher order and thus lower complexity [17] (Supplementary Materials). We also studied the percentage of common and uncommon connections within tiers, following the hypothesis

than adults have more well established network architecture and have more common connections within tiers than neonates (Supplementary Materials).

2.5. Statistical analysis

Wilcoxon rank sum tests were carried out to assess the significance of the differences of distributions of network index values between the structural connectomes and configuration models. The Benjamini-Hochberg false detection rate procedure was carried out across all reported p-values at the strict level of $q = 0.05$. The cut-off of the false detection rate in this study was 0.0264 (i.e. maximum acceptable p-value), which reflects the large proportion of differences found here. The effect sizes were also computed with Cohen's d.

3. Results

3.1. Hierarchical tiers organization

First, we inspected the existence of tiers in the structural connectomes of both term-born and preterm-born neonate groups and adults by considering their group-aggregated degree distributions (i.e. all degrees appearing in all connectomes of the group), Fig 1. The analysis revealed four distinct peaks in the neonatal groups, that were also reflected in the adult connectomes. Further analysis of ROIs in these tiers showed that consistency between neonates and adults was better achieved by consolidating Tier 1 and Tier 2 in neonates as Tier A (incidentally, Tier A corresponds to the rich club community for each population [see Supplementary Materials]), comparable to Tier 1 in adults, and by consolidating Tier 2 and Tier 3 in adults as Tier B, comparable to Tier 3 in neonates. Tier 4 showed high consistency and was relabelled as Tier C. See Supplementary Materials for full details.

We can see the 1 to 4 Tier distributions over the brain for each population in Fig 2 [49]. For this figure, an ROI was generally assigned to a tier if it was included in that tier in at least two thirds of the population. For the A-C Tier distribution see Supplementary Materials.

3.2. Hierarchical complexity

We first assessed the global HC between term-born and preterm-born neonates and adults and the complexity within tiers of the term-born and preterm-born neonates, Fig. 3. HC was significantly larger in term-born neonates than preterm-born neonates ($p = 0.0148, d = 0.3946$). Tier B showed a corresponding significant difference in HC with a stronger effect size ($p = 2.63 \times 10^{-4}, d = 0.6230$), while no difference was evident in any other tier, and thus Tier B could be discerned as the main cause of the global effect.

Global HC of adults was in turn larger than term-born neonates, with over three times the effect size as between preterm- and term-born neonates ($p = 2.63 \times 10^{-11}, d = 1.2859$). To account for the large differences in degree distributions which may impact this finding, we compared each complexity value against those obtained for their corresponding configuration models (networks with the same degree distributions but randomised connections). We conducted this analysis for the adapted tier system to compare similar tiers across neonates and adults. The results are shown in Fig 4. The findings of global HC were confirmed in comparisons with configuration models with term-born connectomes having significantly greater HC than their configuration models, an effect which was not seen in preterm-born connectomes after False Discovery Rate correction FDR). Again an even larger significant difference was seen in adults.

The result of greater complexity in Tier B of term-born neonates was also confirmed in comparisons with configuration models (Tier B in Fig 4). Tier B showed a clear increase of complexity compared to configuration models from preterm- to term-born babies. Interestingly there was also a clearly larger significant difference in adults. Surprisingly, Tier A exhibited lower HC compared to configuration models in all of the groups. This difference was evidently greater for adults compared to neonates. While the effect size was seemingly larger in preterm- to term-born neonates in Tier A, the non-parametric Wilcoxon's rank sum test had a smaller p-value in term-born neonates. This suggested that the clearly visible outliers in the term-born group were behind this discrepancy. Again, this suggested that the trend in term-born neonates moved away from preterm-born neonate connectomes towards adult connectomes. Since configuration models are

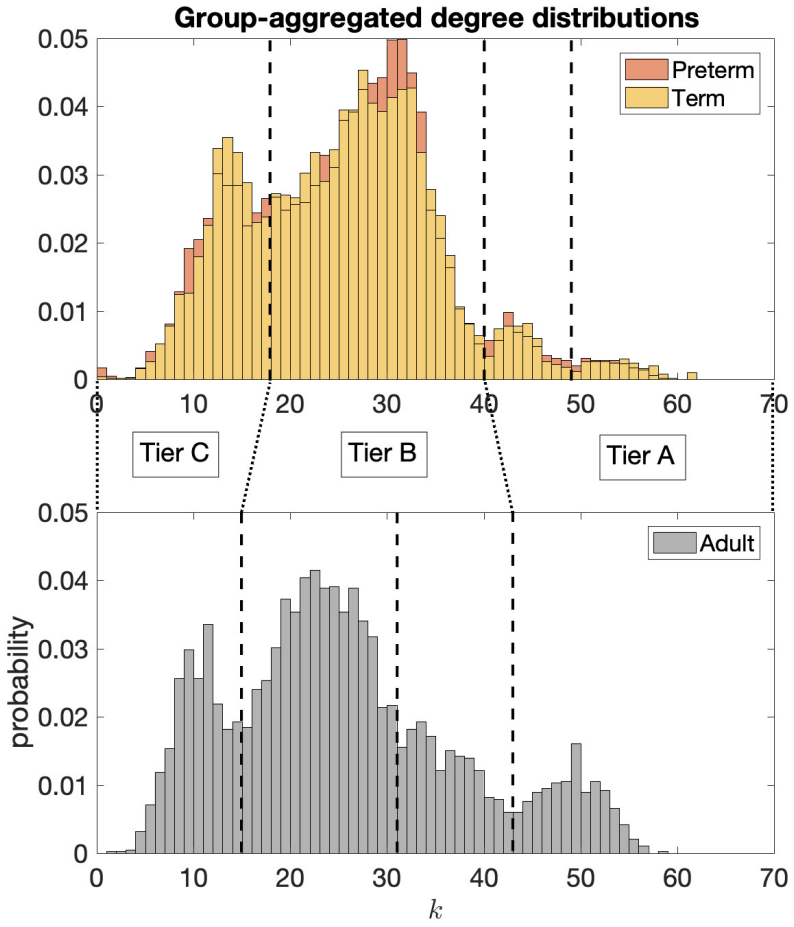

Figure 1: Aggregated degree distributions of neonatal groups, top, and the adult group, bottom. Four distinct peaks are noted in the degree distributions of neonatal connectomes and corresponding peaks are also seen in the adult connectomes. These are taken as the natural tiers and black lines indicating the minima between peaks are taken as the thresholds between tiers. Greater consistency between neonates and adults is found by consolidating the tiers as indicated by Tier A, B and C.

the random case, these results indicate that Tier A is more ordered than expected by random chance and becomes more ordered with maturation, while Tier B is more complex than random chance and becomes more complex with maturation.

3.3. Symmetry and common connections

We hypothesised that the decreasing complexity in Tier A and increasing complexity in Tier B from neonates to adults reflected a systemic change whereby hub nodes create an ordered core structure integrating information from lower order nodes able to specialise into specific functional roles. In this light, we tested two possible contributors to the observed trends of HC: i) the hemispheric symmetry of connectivity patterns, and ii) commonality of ROIs connected to a given tier.

To measure symmetry we analysed the ratio of the average hemispheric symmetry of connections within each tier to the uniformly random expected value. For full details see Supplementary Materials. Table 1 reports the computed symmetry scores comparing the neighbourhoods of homotopic brain regions, averaged by group and by tiers. We observed a consistent behavior across groups of subjects, with Tier A being the

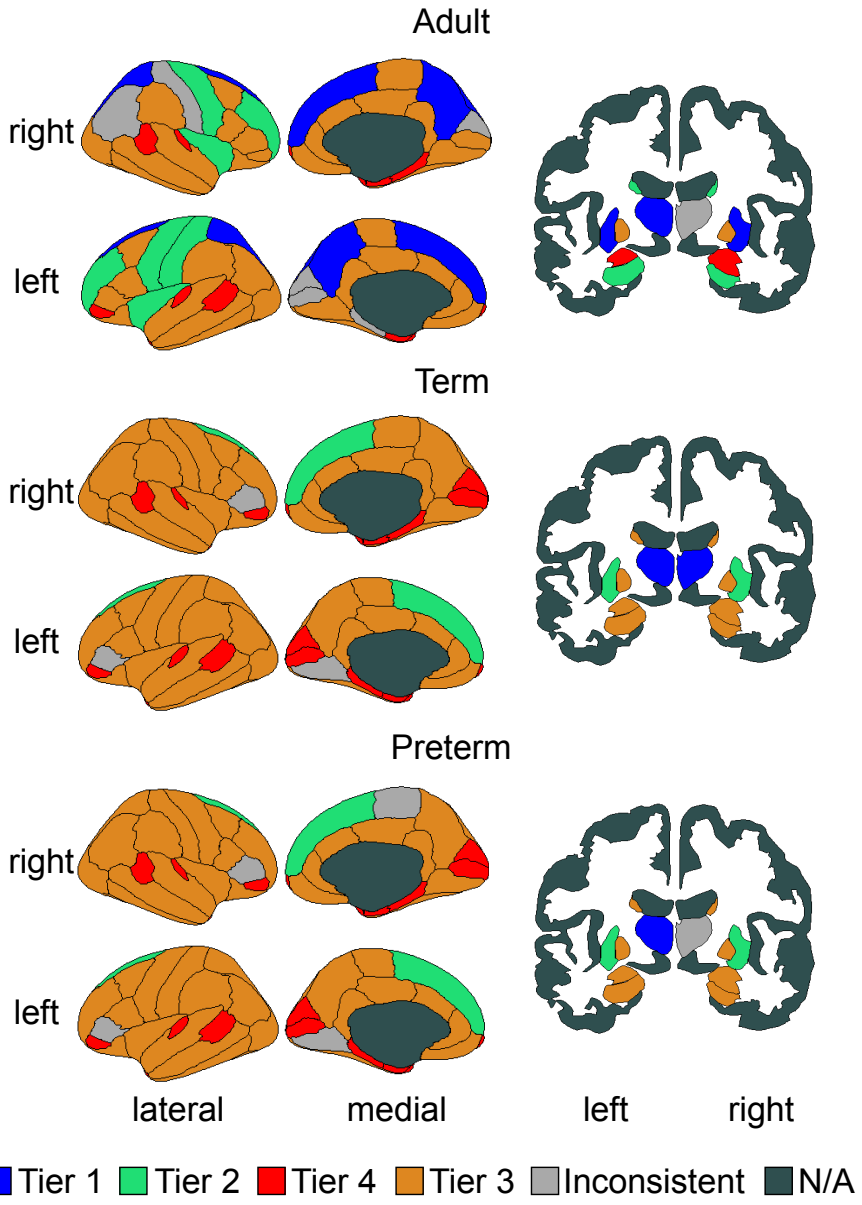

Figure 2: Cortical and sub-cortical representations colored by tiers. N/A means non assigned. Due to the display plane used, two areas are not shown, the accumbens area, that was assigned (in both hemispheres) to Tier 4 in all three populations; and the cerebellum, that was assigned (in both hemispheres) to Tier 3 in all three populations.

most symmetric, and decreasing symmetry from top to bottom tiers. Because it can be expected that nodes with greater degree will have a larger overlap of symmetric connections, just due to having many connections and a limited number of nodes with which to make those connections, we were cautious of interpreting these results as a general pattern. However, in almost all cases the distributions were significantly different between groups. The results suggested that adults in general had less hemispherical symmetry across the connectome. From this, we concluded that hemispheric symmetry was not a strong contributing factor to HC, particularly increased symmetry in Tier A was not evident and not contributing to the observed increased order of Tier A nodes.

Another possible contributing factor to the increased order seen in Tier A and increased complexity seen

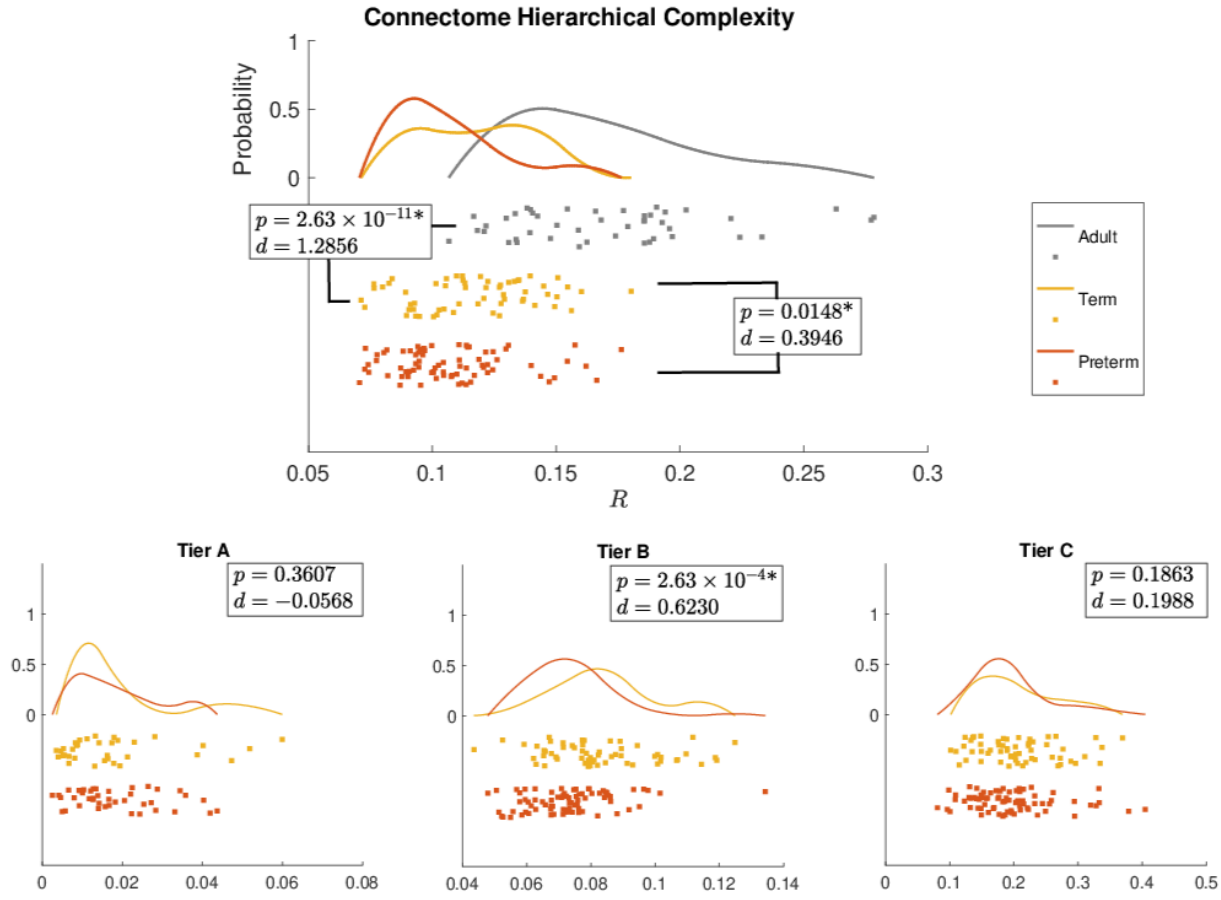

Figure 3: Distribution of the global HC (R) for the three populations as rain cloud plots (top) and HC of the three tiers in neonatal populations (bottom). Wilcoxon rank sum p-values and Cohen's d values are shown for preterm vs term infants (all) and term infants vs adult (top). * denotes significant difference after FDR correction.

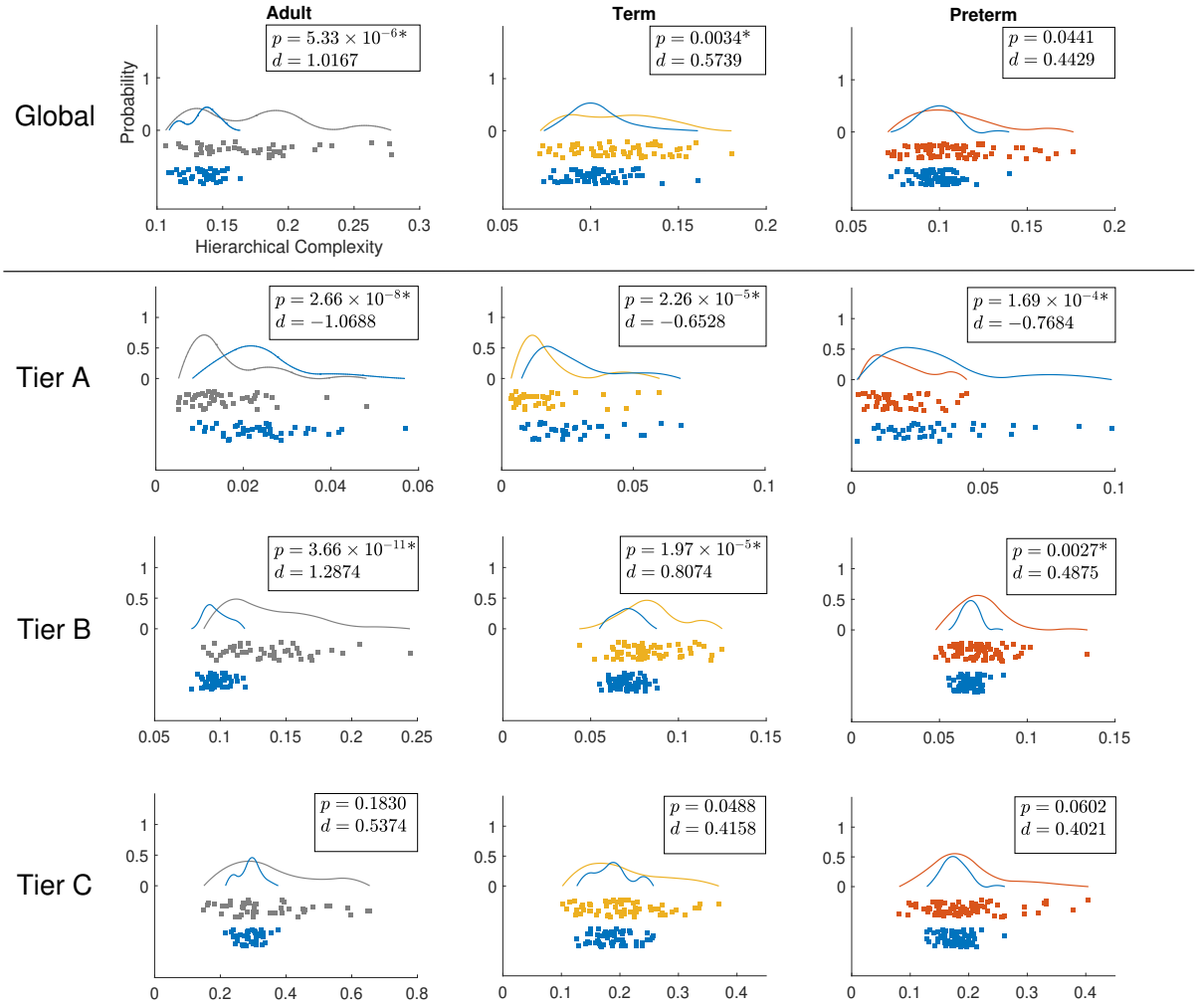

Figure 4: Distributions of HC globally (top) and for the different tiers of the three populations. Grey, yellow and orange colours represent values for adults, term- and preterm-born neonates, respectively, while blue represents the values of HC for their corresponding configuration models. Wilcoxon rank sum p-values and Cohen's d values are shown in top right corner of each plot. Axes as in top left plot. * denotes significant difference after FDR correction.

Table 1: Symmetry scores by tier (mean ± standard deviation) and p-values of group differences from Wilcoxon rank-sum tests. * denotes significant difference after FDR correction.

	symmetry			p-value		
	adult	term	preterm	adult vs term	adult vs preterm	term vs preterm
Tier A	1.81 ± 0.03	1.83 ± 0.03	1.83 ± 0.04	7.01×10^{-5}*	0.0031*	0.2464
Tier B	1.64 ± 0.02	1.70 ± 0.02	1.70 ± 0.02	3.33×10^{-18}*	5.80×10^{-20}*	0.0029*
Tier C	1.24 ± 0.01	1.32 ± 0.02	1.31 ± 0.02	3.14×10^{-18}*	3.91×10^{-20}*	0.0222*

in Tier B would be if all Tier A ROIs tended to connect more to the same ROIs across the connectome while Tier B ROIs tended to exhibit less common connections in adults. To study this, we measured the number of common and uncommon connections made by nodes in each tier. See Table 2 for results (and Supplementary Materials for full details). It was found that Tier A had significantly more common connections for adults than for term born neonates ($p = 3.98 \times 10^{-4}$) who in turn had significantly more common connections than preterm-born neonates ($p = 0.0023$). At the same time, Tier B had significantly more uncommon connections in adults than in neonates ($p = 3.86 \times 10^{-16}$ vs term and $p = 2.62 \times 10^{-19}$ vs preterm) with no statistical difference found between neonate groups ($p = 0.1321$). Tier C showed no differences in uncommon connections between the three groups. These results aligned well with results of HC indicating that common and uncommon connections were a contributing factor.

Table 2: The p-values of group differences from Wilcoxon rank-sum tests between numbers of common and uncommon neighbours of each tier. * denotes significant difference after FDR correction.

	p-value		
	adult vs term	adult vs preterm	term vs preterm
Tier A common	3.98×10^{-4}*	6.48×10^{-11}*	0.0023*
Tier B uncommon	3.86×10^{-16}*	2.62×10^{-19}*	0.1321
Tier C uncommon	0.8850	0.5782	0.6439

4. Discussion

4.1. Tier analysis

Group-aggregated degree distributions revealed the neonatal and adult connectomes comprised of four tiers of connectivity, with a heavy-tailed distribution on the right tail, meaning that there are a few nodes (hubs) that are more densely connected compared to others [7]. The original definition of hierarchical tiers was based on quartiles of the maximum degree, which were defined strictly for purposes of a more fine-grained analysis without any particular hypothesis of functionality [16]. These current findings illuminate why that choice turned out to have evident biological meaning. The four tiers identified by the group-aggregated degree distributions of the adults were of roughly equal-width, thereby coinciding with the quartiles in the original tier definition.

The preterm- and term-born neonates showed an almost identical tier composition although connectivity within tiers indicated a shift to a more unequal degree distribution in term-born neonates with connectivity (indicated by average degree) shifting from Tier 3 to Tiers 4 and 1 from the preterm- to term-born neonate group (see Supplementary Materials), agreeing with previous evidence of decreased 'hub' and 'peripheral' node connections in preterm infants [13]. A very substantial difference in tier composition was noted in the adult connectomes. The regions comprising Tiers 1 and 2 in the neonates were now grouped together in the highest tier of the adults connectome, while the regions comprising Tier 3 in the neonates were broadly split into two distinct tiers in the adult brain. Further, this split was not found to be consistent with the within-tier degree strengths between the neonates and adults. Correlations substantially dropped when comparing the top and bottom halves of Tier 3 in neonates with the split into two tiers in adults (see Supplementary Materials). This indicates a significant rearrangement of these medium degree ROIs in the developing brain.

Tier 1 in neonates was consistently composed solely of the thalamus. The thalamus forms a series of densely-connected processing loops with connectivity that covers large portions of the cortex and with the hippocampus [50, 51, 52]. Among the subcortical regions, the thalamus and its connections are most strongly linked with supporting complex cognitive processes in adults, and appears most strongly susceptible to ageing, partly via vascular risk [53, 54, 55]. In early life, prior work indicates that thalamo-cortical pathways are important for the regulation of area-specific differentiation of the developing brain [6]. The early wave of migrating neurons relay thamalo-cortical projections during late fetal and early preterm development,

the thalamic nuclei may exhibit different maturational trajectories: the posterior limb of the internal capsule (which include the posterior thalamic radiations) appears to develop earlier than the anterior limb (including anterior thalamic pathways [56, 57]). Given that prenatal development of thalamo-cortical connectivity appears to be the time during which the most significant macroscopic changes occur, as observed using dMRI [58], and that preterm infants exhibit reduced corticothalamic connectivity [59], this may partly explain the preterm-term differences in thalamic tier membership (i.e. preterm conditions impact the later-developing pathways and thus a higher degree of connectivity – later maturation – for the thalamus in terms than preterms, where the phases of thalamocortical connectivity may be impeded by interruption of the developmental environment).

Tier 1 in adults, on the other hand, also contained the superior frontal gyrus and putamen (Tier 2 in neonates) as well as the precuneus (Tier 3 in neonates). In general, and as above, the pattern of regional asynchrony in the developmental pattern of WM fiber organisation and myelination may partly explain the differences between neonatal and adult brain hierarchical organisation. WM pathway growth and maturation spans a large time period, from the second half of pregnancy through to late adolescence; during development frontal and temporal WM appears to show the most delayed developmental trajectories in fractional anysotropy (FA) [60], though the authors make it clear that, given FA is likely to be differentially sensitive to the 'local fiber architectural millieu' in neonatal versus adult brains (due to the differential presence of myelin), one should be cautious about directly attributing FA changes to any specific WM characteristic. Given that subcortico-cortical and association fibres (cortico-cortical) especially in the frontal lobes exhibit later maturation [61], it is likely that the shift from Tier 2 to Tier 1 of these regions represents more protracted course of hodological maturation in these areas.

Tier 2 in adults consistently contained the post central, precentral, rostral middle frontal gyrii, and the insulate, caudate and hippocampus. As in previous findings [16], some of these can be broadly classified as lower order sensory processing regions. As above, the fact that there is poorer differentiation between HC tiers in neonates at this stage reflects the fact that there is a huge amount of development still to come. For example, one could conjecture that the developmental period that ensues post-birth, for the next few years in particular, is the time during which there is hierarchical differentiation between these sensory processing regions (Tier 2) and the heteromodal integration regions (Tier 3) that we see in the adult brain. Longitudinal research will be central to testing this hypothesis, and characterising the changes in Tier membership that occur with ongoing early life development.

4.2. Hierarchical complexity

The results on global complexity (Fig. 3) indicate greater HC in the term born brain than the preterm born brain (scanned at term equivalent age). Also, it was found that HC in adults was much greater than in neonates.

From this we can draw two main conclusions. Firstly, HC is affected by prematurity and/or the external stimuli that the preterm babies receive during the first weeks of life. Secondly, HC of the structural connectome develops during childhood and adolescence until reaching the expected values of an adult healthy population. Comparing each population against their configuration model (first row of figure 4), we can see how in preterm connectomes the structure is not yet strongly distinguishable from random, whereas in term born babies, a more complex hierarchical structure is already present. As expected from previous results, this structure is clearly established in the adults [16].

The tier-based analysis revealed that this global difference between term and preterm HC was due to the complexity evident in Tier B regions (figure 3). It is important to notice that Tier B has the largest number of ROIs in term and preterm infants (see Supplementary Materials). At this age, the network segregation/integration balance is still experiencing many changes, including in the transformation of the connectomic architecture from a relatively randomized configuration to a well-organized one [62].

When we compared the Tier against the configuration models, we found that Tier A was less complex than their respective configuration models in all three populations while Tier B was more complex (no differences were found for Tier C), Fig 3. It is interesting to note that there were no differences in Tier A between term and preterm infants. Tier A corresponds to the hubs of the brain, and the lack of difference

indicates that this "core network" is resilient to prematurity. Taken together, these findings are consistent with the hypothesis that term-born infants have a greater cerebral maturation than preterm-born infants, with topological properties going in the direction of the properties displayed by the adult connectomes.

4.3. Symmetry and common connections

We found that connectivity patterns in the adult brain were generally less symmetric than neonates. This is generally consistent with recent findings on cortical metrics that show that most genetic effects on structural variation are shared bilaterally and that asymmetry increases with age [63]. It is reasonable to infer that the same is true of connectivity.

Surprisingly, we found that connectivity patterns in hub regions become more homogeneous with age and consistently more homogeneous than expected due to random chance. The fronto-parietal network has long been associated with higher cognitive processes such as general intelligence [64, 55]. As such, it may be that postnatal development is important for establishing the emergent association fibre development that facilitates this networks' putative support for higher order cognitive abilities.

The symmetry analysis and the comparison of common and uncommon connections lead us to one conclusion: hub regions become less symmetric in adults, while at the same time the connectivity patterns over all hub regions become more homogeneous.

4.4. Previous work

Comparing neonatal structural connectivity studies is very difficult, due to the lack of a standarized protocol for dMRI processing, parcellation or network analysis (for a review on the topic please see Zhao et al. [65]). In the literature, an increased clustering coefficient, modularity, local and global efficiency and reduced characteristic shortest path length have been found when comparing term-born against preterm-born infants [66, 13, 8, 67, 9]. This results in the network becoming more efficiently connected with development in terms of both network integration and segregation [65]. However, all these studies were performed scanning the preterm children when they are born. From our knowledge, only two studies compare term- with preterm-born infants scanned at term equivalent age: Ball et al. [13] and Lee et al. [11]. Their findings were consistent: an increased small-worldness in Lee et al. [11] and an increased clustering coefficient in Ball et al. [13] in preterm infants at term equivalent age. This suggests that the structural brain network after preterm birth is reorganized in maximizing integrated and segregated processing, implying resilience against prematurity associated pathology [11]. Our findings also point to this direction, there is at least a part of the network – the main core/hubs (Tier A) – that is resilient to prematurity and at term equivalent age is not different between term and preterm infants.

Early life adversity (such as preterm birth) can impact the development of brain networks by modulating synaptic maturation and pruning among other effects. Although the general framework of brain circuits is dictated by genes and is in place by the time of birth [68], the emerging brain networks are still immature, and chaotic unpredictable patterns of experiential signals from the environment can disrupt normal maturation [69]. Accumulating evidence from imaging studies supports the theory that preterm birth affects brain growth and cortical maturation: reduced WM and GM volumes, altered microstructure and atypical connectivity patterns [1], both at the global level and in specific networks such as the thalamocortical system [70, 6] and regions supporting neurocognitive and primary motor/sensory functions [71], all suggest a delayed or atypical maturation associated with prematurity. Our results, showing a reduced HC in preterm- compared with term-born infants, corroborate this hypothesis and move towards providing a framework within which to observe and understand the developing brain as a complex hierarchical system.

5. Conclusion

This study provides a new systems-level paradigm to understand the macro-scale developing brain. It is the first to consider the existence and implications of hierarchical tiers and their contingent connectivity patterns in the neonatal brain. We found that HC was greater in term-born neonates than in preterm infants, the latter of which, indeed, could not be statistically distinguished from randomised configuration

models. Natural tiers were discovered in the group-aggregated connectome degree distributions, with clear reconfigurations occurring between neonates and adults in high level and intermediate tiers. The difference in complexity between neonatal groups was found to be driven by neonatal Tier B, comprising regions –which later split into two distinct tiers in adults – involving sensorimotor processing and regions integrating high order cognitive and lower order sensorimotor processing. Comparisons with configuration models revealed a hierarchical structure where top tier hub regions were less complex (thus more ordered) than expected by random chance while Tier 3 regions were more complex than expected by random chance with statistical results indicating these patterns were dysmature in preterm-born neonates. The former result was at least partly due to common ROIs to which hub regions connected, with the superior frontal gyrus, putamen and precuneus joining the thalamus as hubs in adults. The latter on the other hand, indicated the beginnings of specialisation of multifarious cortical regions in neonates, with greater specialisation observed in term-born neonates. We have demonstrated the potential of this approach in a study of preterm birth, but these concepts can be applied in more general settings to understand the neural bases of cognition in health and disease. A natural extension of this work would be analysis of the developmental trajectory of HC across childhood and adolescence, and its variability in older age. This would allow the investigation of deviations from normal progression associated with cognitive impairment, and any brain disorder in early or later life that is characterised by alterations in network topology and global connectivity patterns.

Data availability

The HC code can be found in [72]. Reasonable requests for original image data will be considered through the BRAINS governance process (`www.brainsimagebank.ac.uk`) [73].

Acknowledgements

Adult datasets were provided by the Human Connectome Project, WU-Minn Consortium (Principal Investigators: David Van Essen and Kamil Ugurbil; 1U54MH091657) funded by the 16 NIH Institutes and Centers that support the NIH Blueprint for Neuroscience Research; and by the McDonnell Center for Systems Neuroscience at Washington University. Individual parcellated templates and structural MRI images from the M-CRIB atlas [28] were supplied by the Murdoch Children's Research Institute. This work was supported by Theirworld (www.theirworld.org) and by Health Data Research UK (MRC ref Mr/S004122/1), which is funded by the UK Medical Research Council, Engineering and Physical Sciences Research Council, Economic and Social Research Council, National Institute for Health Research (England), Chief Scientist Office of the Scottish Government Health and Social Care Directorates, Health and Social Care Research and Development Division (Welsh Government), Public Health Agency (Northern Ireland), British Heart Foundation and Wellcome. MJT was supported by NHS Lothian Research and Development Office. Part of the work was undertaken in the MRC Centre for Reproductive Health, which is funded by MRC Centre Grant (MRC G1002033). SRC was supported by the MRC (MR/R024065/1) and National Institutes of Health (R01AG054628). Neonatal participants were scanned in the University of Edinburgh Imaging Research MRI Facility at the Royal Infirmary of Edinburgh which was established with funding from The Wellcome Trust, Dunhill Medical Trust, Edinburgh and Lothians Research Foundation, Theirworld, The Muir Maxwell Trust and many other sources. We are grateful to the families who consented to take part in the study and to all the University's imaging research staff for providing the infant scanning.

References

[1] J. P. Boardman, S. J. Counsell, Invited review: Factors associated with atypical brain development in preterm infants: insights from magnetic resonance imaging, Neuropathology and Applied Neurobiology n/a (n/a) (2019). `arXiv:https://onlinelibrary.wiley.com/doi/pdf/10.1111/nan.12589`, `doi:10.1111/nan.12589`.
URL `https://onlinelibrary.wiley.com/doi/abs/10.1111/nan.12589`

[2] C. Nosarti, A. Reichenberg, R. M. Murray, S. Cnattingius, M. P. Lambe, L. Yin, J. MacCabe, L. Rifkin, C. M. Hultman, Preterm Birth and Psychiatric Disorders in Young Adult Life, Archives of General Psychiatry 69 (6) (2012) 610–617 (2012).

[3] K. Mathewson, C. Chow, K. Dobson, E. Pope, L. Schmidt, R. Van Lieshout, Mental health of extremely low birth weight survivors: A systematic review and meta-analysis., Psychological Bulletin 143 (4) (2017) 347 – 383 (2017).

[4] D. Wolke, S. Johnson, M. Mendonça, The life course consequences of very preterm birth, Annual Review of Developmental Psychology 1 (1) (2019) 69–92 (2019). arXiv:https://doi.org/10.1146/annurev-devpsych-121318-084804, doi:10.1146/annurev-devpsych-121318-084804.
URL https://doi.org/10.1146/annurev-devpsych-121318-084804

[5] D. Batalle, A. D. Edwards, J. O'Muircheartaigh, Annual research review: Not just a small adult brain: understanding later neurodevelopment through imaging the neonatal brain, Journal of Child Psychology and Psychiatry 59 (4) (2018b) 350–371 (2018b). doi:10.1111/jcpp.12838.

[6] G. Ball, J. P. Boardman, P. Aljabar, A. Pandit, T. Arichi, N. Merchant, D. Rueckert, A. D. Edwards, S. J. Counsell, The influence of preterm birth on the developing thalamocortical connectome, Cortex 49 (6) (2013) 1711 – 1721 (2013). doi:https://doi.org/10.1016/j.cortex.2012.07.006.

[7] M. P. Van Den Heuvel, K. J. Kersbergen, M. A. De Reus, K. Keunen, et al., The neonatal connectome during preterm brain development, Cerebral Cortex 25 (9) (2015) 3000–3013 (2015). doi:10.1093/cercor/bhu095.

[8] C. J. Brown, S. P. Miller, B. G. Booth, S. Andrews, V. Chau, K. J. Poskitt, G. Hamarneh, Structural network analysis of brain development in young preterm neonates, NeuroImage 101 (2014) 667 – 680 (2014). doi:https://doi.org/10.1016/j.neuroimage.2014.07.030.

[9] D. Batalle, E. J. Hughes, H. Zhang, J.-D. Tournier, N. Tusor, others., Early development of structural networks and the impact of prematurity on brain connectivity, NeuroImage 149 (2017) 379–392 (2017). doi:10.1016/j.neuroimage.2017.01.065.

[10] T. Zhao, V. Mishra, T. Jeon, M. Ouyang, Q. Peng, L. Chalak, J. L. Wisnowski, R. Heyne, N. Rollins, N. Shu, H. Huang, Structural network maturation of the preterm human brain, NeuroImage 185 (2019) 699 – 710 (2019). doi:https://doi.org/10.1016/j.neuroimage.2018.06.047.
URL http://www.sciencedirect.com/science/article/pii/S1053811918305548

[11] J. Lee, H. Park, H. Lee, Accelerated small-world property of structural brain networks in preterm infants at term-equivalent age., Neonatology 115 (2019) 99–107 (2019). doi:https://doi.org/10.1159/000493087.

[12] P. Galdi, M. Blesa, D. Q. Stoye, G. Sullivan, G. J. Lamb, A. J. Quigley, M. J. Thrippleton, M. E. Bastin, J. P. Boardman, Neonatal morphometric similarity mapping for predicting brain age and characterizing neuroanatomic variation associated with preterm birth, bioRxiv (2019). arXiv:https://www.biorxiv.org/content/early/2019/03/07/569319.full.pdf, doi:10.1101/569319.
URL https://www.biorxiv.org/content/early/2019/03/07/569319

[13] G. Ball, P. Aljabar, S. Zebari, N. Tusor, T. Arichi, N. Merchant, E. C. Robinson, E. Ogundipe, D. Rueckert, A. D. Edwards, S. J. Counsell, Rich-club organization of the newborn human brain, Proceedings of the National Academy of Sciences 111 (20) (2014) 7456–7461 (2014). arXiv:https://www.pnas.org/content/111/20/7456.full.pdf, doi:10.1073/pnas.1324118111.
URL https://www.pnas.org/content/111/20/7456

[14] E. J. Telford, S. R. Cox, S. Fletcher-Watson, D. Anblagan, S. Sparrow, R. Pataky, A. Quigley, S. I. Semple, M. E. Bastin, J. P. Boardman, A latent measure explains substantial variance in white matter microstructure across the newborn human brain, Brain Structure and Function 222 (9) (2017) 4023–4033 (Dec 2017). doi:10.1007/s00429-017-1455-6.
URL https://doi.org/10.1007/s00429-017-1455-6

[15] S. Stoecklein, A. Hilgendorff, M. Li, K. Förster, A. W. Flemmer, F. Galiè, S. Wunderlich, D. Wang, S. Stein, H. Ehrhardt, O. Dietrich, Q. Zou, S. Zhou, B. Ertl-Wagner, H. Liu, Variable functional connectivity architecture of the preterm human brain: Impact of developmental cortical expansion and maturation, Proceedings of the National Academy of Sciences (2019). arXiv:https://www.pnas.org/content/early/2019/12/26/1907892117.full.pdf, doi:10.1073/pnas.1907892117.
URL https://www.pnas.org/content/early/2019/12/26/1907892117

[16] K. Smith, M. Bastin, S. Cox, M. Valdes-Hernandez, S. Wiseman, J. Escudero, C. Sudlow, Hierarchical complexity of the adult human structural connectome, Neuroimage 191 (2019) 205–215 (2019).

[17] K. Smith, On neighbourhood degree sequences of complex networks, Scientific Reports 9 (2019) 8340 (2019).

[18] E. Caruyer, C. Lenglet, G. Sapiro, R. Deriche, Design of multishell sampling schemes with uniform coverage in diffusion MRI, Magnetic Resonance in Medicine 69 (6) (2013) 1534–1540 (2013). doi:10.1002/mrm.24736.

[19] D. V. Essen, K. Ugurbil, E. Auerbach, D. Barch, T. Behrens, R. Bucholz, A. Chang, L. Chen, M. Corbetta, S. Curtiss, S. D. Penna, D. Feinberg, M. Glasser, N. Harel, A. Heath, L. Larson-Prior, D. Marcus, G. Michalareas, S. Moeller, R. Oostenveld, S. Petersen, F. Prior, B. Schlaggar, S. Smith, A. Snyder, J. Xu, E. Yacoub, The human connectome project: A data acquisition perspective, NeuroImage 62 (4) (2012) 2222 – 2231, connectivity (2012). doi:https://doi.org/10.1016/j.neuroimage.2012.02.018.
URL http://www.sciencedirect.com/science/article/pii/S1053811912001954

[20] J. Veraart, D. S. Novikov, D. Christiaens, B. Ades-aron, J. Sijbers, E. Fieremans, Denoising of diffusion MRI using random matrix theory, NeuroImage 142 (2016b) 394–406 (2016b). doi:10.1016/j.neuroimage.2016.08.016.

[21] J. L. Andersson, S. Skare, J. Ashburner, How to correct susceptibility distortions in spin-echo echo-planar images: application to diffusion tensor imaging, NeuroImage 20 (2) (2003) 870 – 888 (2003). doi:https://doi.org/10.1016/S1053-8119(03)00336-7.

[22] J. L. Andersson, S. N. Sotiropoulos, An integrated approach to correction for off-resonance effects and subject movement in diffusion MR imaging, NeuroImage 125 (2016) 1063–1078 (2016). doi:10.1016/j.neuroimage.2015.10.019.

[23] J. L. Andersson, M. S. Graham, E. Zsoldos, S. N. Sotiropoulos, Incorporating outlier detection and replacement into a non-parametric framework for movement and distortion correction of diffusion MR images, NeuroImage 141 (2016) 556–572 (2016). doi:10.1016/j.neuroimage.2016.06.058.

[24] J. L. Andersson, M. S. Graham, I. Drobnjak, H. Zhang, N. Filippini, M. Bastiani, Towards a comprehensive framework for movement and distortion correction of diffusion MR images: Within volume movement, NeuroImage 152 (2017) 450–466 (2017). doi:10.1016/j.neuroimage.2017.02.085.

[25] N. J. Tustison, B. B. Avants, P. A. Cook, Y. Zheng, A. Egan, P. A. Yushkevich, J. C. Gee, N4ITK: Improved N3 bias correction, IEEE Transactions on Medical Imaging 29 (6) (2010) 1310–1320 (2010). doi:10.1109/TMI.2010.2046908.

[26] A. Makropoulos, I. S. Gousias, C. Ledig, P. Aljabar, A. Serag, J. V. Hajnal, A. D. Edwards, S. J. Counsell, D. Rueckert, Automatic whole brain MRI segmentation of the developing neonatal brain, IEEE Transactions on Medical Imaging 33 (9) (2014) 1818–1831 (2014). doi:10.1109/TMI.2014.2322280.

[27] A. Makropoulos, E. C. Robinson, A. Schuh, R. Wright, S. Fitzgibbon, et al., The developing human connectome project: A minimal processing pipeline for neonatal cortical surface reconstruction, NeuroImage 173 (2018) 88–112 (2018). doi:10.1016/j.neuroimage.2018.01.054.

[28] B. Alexander, A. L. Murray, W. Y. Loh, L. G. Matthews, C. Adamson, R. Beare, J. Chen, C. E. Kelly, S. Rees, S. K. Warfield, P. J. Anderson, L. W. Doyle, A. J. Spittle, J. L. Cheong, M. L. Seal, D. K. Thompson, A new neonatal cortical and subcortical brain atlas: the melbourne children's regional infant brain (m-crib) atlas, NeuroImage 147 (2017) 841 – 851 (2017). doi:https://doi.org/10.1016/j.neuroimage.2016.09.068.
URL http://www.sciencedirect.com/science/article/pii/S1053811916305444

[29] B. Avants, C. Epstein, M. Grossman, J. Gee, Symmetric diffeomorphic image registration with cross-correlation: Evaluating automated labeling of elderly and neurodegenerative brain, Medical Image Analysis 12 (1) (2008) 26 – 41, special Issue on The Third International Workshop on Biomedical Image Registration – WBIR 2006 (2008). doi:https://doi.org/10.1016/j.media.2007.06.004.
URL http://www.sciencedirect.com/science/article/pii/S1361841507000606

[30] H. Wang, J. W. Suh, S. R. Das, J. B. Pluta, C. Craige, P. A. Yushkevich, Multi-atlas segmentation with joint label fusion, IEEE Transactions on Pattern Analysis and Machine Intelligence 35 (3) (2013) 611–623 (2013). doi:10.1109/TPAMI.2012.143.

[31] D. N. Greve, B. Fischl, Accurate and robust brain image alignment using boundary-based registration, NeuroImage 48 (1) (2009) 63–72 (2009). doi:10.1016/j.neuroimage.2009.06.060.

[32] M. F. Glasser, S. N. Sotiropoulos, J. A. Wilson, T. S. Coalson, B. Fischl, J. L. Andersson, J. Xu, S. Jbabdi, M. Webster, J. R. Polimeni, D. C. V. Essen, M. Jenkinson, The minimal preprocessing pipelines for the human connectome project, NeuroImage 80 (2013) 105 – 124, mapping the Connectome (2013). doi:https://doi.org/10.1016/j.neuroimage.2013.04.127.
URL http://www.sciencedirect.com/science/article/pii/S1053811913005053

[33] S. N. Sotiropoulos, S. Jbabdi, J. Xu, J. L. Andersson, S. Moeller, E. J. Auerbach, M. F. Glasser, M. Hernandez, G. Sapiro, M. Jenkinson, D. A. Feinberg, E. Yacoub, C. Lenglet, D. C. V. Essen, K. Ugurbil, T. E. Behrens, Advances in diffusion mri acquisition and processing in the human connectome project, NeuroImage 80 (2013) 125 – 143, mapping the Connectome (2013). doi:https://doi.org/10.1016/j.neuroimage.2013.05.057.
URL http://www.sciencedirect.com/science/article/pii/S105381191300551X

[34] R. S. Desikan, F. Ségonne, B. Fischl, B. T. Quinn, B. C. Dickerson, D. Blacker, R. L. Buckner, A. M. Dale, R. P. Maguire, B. T. Hyman, M. S. Albert, R. J. Killiany, An automated labeling system for subdividing the human cerebral cortex on mri scans into gyral based regions of interest, NeuroImage 31 (3) (2006) 968 – 980 (2006). doi:https://doi.org/10.1016/j.neuroimage.2006.01.021.
URL http://www.sciencedirect.com/science/article/pii/S1053811906000437

[35] Y. Zhang, M. Brady, S. Smith, Segmentation of brain mr images through a hidden markov random field model and the expectation-maximization algorithm, IEEE Transactions on Medical Imaging 20 (1) (2001) 45–57 (2001). doi:10.1109/42.906424.

[36] B. Patenaude, S. M. Smith, D. N. Kennedy, M. Jenkinson, A bayesian model of shape and appearance for subcortical brain segmentation, NeuroImage 56 (3) (2011) 907 – 922 (2011). doi:https://doi.org/10.1016/j.neuroimage.2011.02.046.
URL http://www.sciencedirect.com/science/article/pii/S1053811911002023

[37] J.-D. Tournier, F. Calamante, A. Connelly, Robust determination of the fibre orientation distribution in diffusion mri: Non-negativity constrained super-resolved spherical deconvolution, NeuroImage 35 (4) (2007) 1459 – 1472 (2007). doi:https://doi.org/10.1016/j.neuroimage.2007.02.016.
URL http://www.sciencedirect.com/science/article/pii/S1053811907001243

[38] T. Dhollander, D. Raffelt, A. Connelly., Unsupervised 3-tissue response function estimation from single-shell or multi-shell diffusion mr data without a co-registered t1 image., in: ISMRM Workshop on Breaking the Barriers of Diffusion MRI., 2016 (2016).

[39] B. Jeurissen, J.-D. Tournier, T. Dhollander, A. Connelly, J. Sijbers, Multi-tissue constrained spherical deconvolution for improved analysis of multi-shell diffusion mri data, NeuroImage 103 (2014) 411 – 426 (2014). doi:https://doi.org/10.1016/j.neuroimage.2014.07.061.
URL http://www.sciencedirect.com/science/article/pii/S1053811914006442

[40] D. Raffelt, T. Dhollander, J.-D. Tournier, R. Tabbara, R. E. Smith, E. Pierre, A. Connelly., Bias field correction and intensity normalisation for quantitative analysis of apparent fiber density., in: Proceedings of the ISMRM., 2018 (2018).

[41] J. D. Tournier, F. Calamante, A. Connelly., Improved probabilistic streamlines tractography by 2nd order integration over fibre orientation distributions., in: Proceedings of the ISMRM., 2010 (2010).

[42] R. E. Smith, J.-D. Tournier, F. Calamante, A. Connelly, Anatomically-constrained tractography: Improved diffusion mri streamlines tractography through effective use of anatomical information, NeuroImage 62 (3) (2012) 1924 – 1938 (2012). doi:https://doi.org/10.1016/j.neuroimage.2012.06.005.
URL http://www.sciencedirect.com/science/article/pii/S1053811912005824

[43] R. E. Smith, J.-D. Tournier, F. Calamante, A. Connelly, Sift2: Enabling dense quantitative assessment of brain white matter connectivity using streamlines tractography, NeuroImage 119 (2015) 338 – 351 (2015). doi:https://doi.org/10.1016/j.neuroimage.2015.06.092.
URL http://www.sciencedirect.com/science/article/pii/S1053811915005972

[44] R. E. Smith, J.-D. Tournier, F. Calamante, A. Connelly, The effects of sift on the reproducibility and biological accuracy of the structural connectome, NeuroImage 104 (2015) 253 – 265 (2015). doi:https://doi.org/10.1016/j.neuroimage.2014.10.004.
URL http://www.sciencedirect.com/science/article/pii/S1053811914008155

[45] C.-H. Yeh, R. E. Smith, T. Dhollander, F. Calamante, A. Connelly, Connectomes from streamlines tractography: Assigning streamlines to brain parcellations is not trivial but highly consequential, NeuroImage (2019). doi:https://doi.org/10.1016/j.neuroimage.2019.05.005.
URL http://www.sciencedirect.com/science/article/pii/S105381191930388X

[46] C. R. Buchanan, M. E. Bastin, S. J. Ritchie, D. C. Liewald, J. W. Madole, E. M. Tucker-Drob, I. J. Deary, S. R. Cox, The effect of network thresholding and weighting on structural brain networks in the uk biobank, NeuroImage (2020) 116443 (2020). doi:https://doi.org/10.1016/j.neuroimage.2019.116443.
URL http://www.sciencedirect.com/science/article/pii/S1053811919310341

[47] K. Smith, J. Escudero, The complex hierarchical topology of eeg functional connectivity, Journal of Neuroscience Methods 276 (2017) 1–12 (2017).

[48] S. Maslov, K. Sneppen, Specificity and stability in topology of protein networks, Science 910 (2002) LP–913 (2002).

[49] A. M. Mowinckel, D. Vidal-Piñeiro, Visualisation of brain statistics with r-packages ggseg and ggseg3d (2019). arXiv:1912.08200.

[50] T. Behrens, H. Johansen-Berg, M. Woolrich, S. Smith, C. Wheeler-Kingshott, P. Boulby, G. Barker, E. Sillery, K. Sheehan, O. Ciccarelli, A. Thompson, J. Brady, P. Matthews, Non-invasive mapping of connections between human thalamus and cortex using diffusion imaging, Nature Neuroscience 6 (2003) 750–757 (2003).

[51] E. Grant, A. Hoerder-Suabedissen, Z. Molnaŕ, Development of the corticothalamic projections, Frontiers in Neuroscience 6 (2012) 53 (2012).

[52] J. P. Aggleton, S. M. O'Mara, S. D. Vann, N. F. Wright, M. Tsanov, J. T. Erichsen, Hippocampal–anterior thalamic pathways for memory: uncovering a network of direct and indirect actions, European Journal of Neuroscience 31 (2010) 2292–2307 (2010).

[53] S. Cox, S. J. Ritchie, E. M. Tucker-Drob, D. C. Liewald, S. P. Hagenaars, G. Davies, J. M. Wardlaw, C. R. Gale, M. E. B. . I. J. Deary, Ageing and brain white matter miscrostructure in 3,513 uk biobank participants, Nature Communications 7 (2016) 13629 (2016).

[54] S. Cox, S. Ritchie, C. Fawns-Ritchie, E. Tucker-Drob, I. Deary, Structural brain imaging correlates of general intelligence in uk biobank, Intelligence 76 (2019) 101376 (2019).

[55] S. Cox, D. Lyall, S. Ritchie, M. Bastin, M. Harris, C. Buchanan, C. Fawns-Ritchie, M. Barbu, L. de Nooij, L. Reus, C. Alloza, X. Shen, E. Neilson, H. Alderson, S. Hunter, D. Liewald, H. Whalley, A. McIntosh, S. Lawrie, J. Pell, E. Tucker-Drob, J. Wardlaw, C. Gale, I. Deary, Associations between vascular risk factors and brain mri indices in uk biobank, European Heart Journal 40 (28) (2019) 2290–2300 (2019).

[56] L. Hermoye, C. Saint-Martin, G. Cosnard, S.-K. Lee, J. Kim, M.-C. Nassogne, R. Menten, P. Clapuyt, P. K. Donohue, K. Hua, S. Wakana, H. Jiang, P. C. van Zijl, S. Mori, Pediatric diffusion tensor imaging: normal database and observation of the white matter maturation in early childhood, Neuroimage 29 (2006) 493–504 (2006).

[57] J. Dubois, G. Dehaene-Lambertz, S. Kulikova, C. Poupon, P. Hüppi, L. Hertz-Pannier, The early development of brain white matter: a review of imaging studies in fetuses, newborns and infants, Neuroscience 276 (2014) 48–71 (2014).

[58] M. Wilkinson, T. Kane, R. Wang, E. Takahashi, Migration pathways of thalamic neurons and development of thalamocortical connections in humans revealed by diffusion mr tractography, Cerebral Cortex 27 (12) (2017) 5683–5695 (2017).

[59] H. Toulmin, C. Beckmann, J. O'Muircheartaigh, G. Ball, P. Nongena, A. Makropoulos, A. Ederies, S. Counsell, N. Kennea, T. Arichi, N. Tusor, M. Rutherford, D. Azzopardi, N. Gonzalez-Cinca, J. Hajnal, E. A.D., Specialization and integration of functional thalamocortical connectivity in the human infant, PNAS 112 (20) (2015) 6485–6490 (2015).

[60] S. Deoni, D. Dean, D. H. O'Muircheartaigh, J., B. Jerskey, Investigating white matter development in infancy and early childhood using myelin water faction and relaxation time mapping, Neuroimage 63 (3) (2012) 1038–1053 (2012).

[61] J. Young, B. Morgan, H. Whyte, W. Lee, M. Smith, C. Raybaud, M. Shroff, J. Sled, M. Taylor, Longitudinal study of white matter development and outcomes in children born very preterm, Cerebral Cortex 27 (8) (2017) 4096–4105 (2017).

[62] M. Cao, H. Huang, Y. He, Developmental connectomics from infancy through early childhood, Trends in Neurosciences 40 (8) (2017) 494 – 506 (2017). doi:https://doi.org/10.1016/j.tins.2017.06.003. URL http://www.sciencedirect.com/science/article/pii/S0166223617301157

[63] X.-Z. Kong, S. Mathias, T. Guadalupe, D. Glahn, B. Franke, F. Crivello, N. Tzourio-Mazoyer, S. Fisher, P. Thompson, C. Francks, Mapping cortical brain asymmetry in 17,141 healthy individuals worldwide via the enigma consortium, PNAS 115 (22) (2018) E5154–E5163 (2018).

[64] H. R. Jung, R.E., The parieto-frontal integration theory (p-fit) of intelligence: converging neuroimaging evidence, Behavioural and Brain Sciences 30 (2) (2007) 135–154 (2007).

[65] T. Zhao, Y. Xu, Y. He, Graph theoretical modeling of baby brain networks, NeuroImage 185 (2019) 711 – 727 (2019). doi:https://doi.org/10.1016/j.neuroimage.2018.06.038.
URL http://www.sciencedirect.com/science/article/pii/S1053811918305457

[66] O. Tymofiyeva, C. P. Hess, E. Ziv, P. N. Lee, H. C. Glass, D. M. Ferriero, A. J. Barkovich, D. Xu, A dti-based template-free cortical connectome study of brain maturation, PLOS ONE 8 (5) (2013) 1–10 (05 2013). doi:10.1371/journal.pone.0063310.
URL https://doi.org/10.1371/journal.pone.0063310

[67] M. P. van den Heuvel, K. J. Kersbergen, M. A. De Reus, K. Keunen, R. S. R. S. Kahn, F. Groenendaal, L. S. De Vries, M. J. Benders, The neonatal connectome during preterm brain development, Cerebral Cortex 25 (9) (2015) 3000–3013 (2015). doi:10.1093/cercor/bhu095.

[68] K. Keunen, S. J. Counsell, M. J. Benders, The emergence of functional architecture during early brain development, NeuroImage 160 (2017) 2–14 (2017). doi:10.1016/J.NEUROIMAGE.2017.01.047.

[69] A. K. Short, T. Z. Baram, Early-life adversity and neurological disease: age-old questions and novel answers, Nature Reviews Neurology (2019) 1–13 (2019).

[70] J. P. Boardman, S. J. Counsell, D. Rueckert, O. Kapellou, K. K. Bhatia, P. Aljabar, J. Hajnal, J. M. Allsop, M. A. Rutherford, A. D. Edwards, Abnormal deep grey matter development following preterm birth detected using deformation-based morphometry, NeuroImage 32 (1) (2006) 70–78 (2006). doi:https://doi.org/10.1016/j.neuroimage.2006.03.029.

[71] M. Bouyssi-Kobar, M. Brossard-Racine, M. Jacobs, J. Murnick, T. Chang, C. Limperopoulos, Regional microstructural organization of the cerebral cortex is affected by preterm birth, NeuroImage: Clinical 18 (2018) 871–880 (2018). doi:10.1016/j.nicl.2018.03.020.

[72] K. M. Smith, Data for: Hierarchical complexity of the adult human structural connectome, https://data.mendeley.com/datasets/758t7h48m7/1 (2019).
URL http://dx.doi.org/10.17632/758t7h48m7.1#file-f9858b97-d99e-4840-af9e-c29d281a0963

[73] D. E. Job, D. A. Dickie, D. Rodriguez, A. Robson, S. Danso, C. Pernet, M. E. Bastin, J. P. Boardman, A. D. Murray, T. Ahearn, G. D. Waiter, R. T. Staff, I. J. Deary, S. D. Shenkin, J. M. Wardlaw, A brain imaging repository of normal structural mri across the life course: Brain images of normal subjects (brains), NeuroImage 144 (2017) 299 – 304, data Sharing Part II (2017). doi:https://doi.org/10.1016/j.neuroimage.2016.01.027.
URL http://www.sciencedirect.com/science/article/pii/S1053811916000331